JOURNAL OF MATERIALS SCIENCE 35 (2000) 4121–4127

Hydrogen transport and environmental embrittlement effects in iron aluminides

W. C. LUU, J. K. WU
Institute of Materials Engineering, National Taiwan Ocean University, Keelung, Taiwan 20224, ROC

Environmental embrittlement types of six iron aluminides have been systematically evaluated using electrochemical hydrogen permeation measurement, hydrogen microprint technique and tensile test in this study. The results of hydrogen permeation and microprint technique show that three α - disordered solid solution structure of binary and ternary iron aluminides (Fe-10Al, Fe-18Al, and Fe-18Al-5Cr) have higher effective diffusivity and permeation rate than B2 ordered structure of binary and ternary iron aluminides (Fe-28Al, Fe-28Al-5Cr, and Fe-40Al). The tensile test of six iron aluminides in air, vacuum treatment and hydrogen precharged were analyzed and concluded. Three α - disordered solid solution structure of iron aluminides suffer in hydrogen environment which are quite different embrittlement mechanisms from those B2 ordered structure of iron aluminides with serious tensile loss in air by moisture induced embrittlement.

1. Introduction

Fe-Al intermetallics are candidates for high temperature applications due to their good tensile strength, low density and excellent oxidation and sulphidation resistance [1]. However, they exhibit poor ambient temperature ductility due to moisture induced hydrogen embrittlement [2–16]. Hydrogen is produced by the reaction of moisture with the iron aluminide and enters the crack tip, or the near the tip area, lower the bonding strength of low index planes or grain boundaries causing brittle fracture [17]. Therefore, one of the important factors that needs to be understood is the hydrogen transport in iron aluminides.

The application of hydrogen microprint technique to study hydrogen distribution in alloy steels has been well developed [18–20], and is proving to be very simple and accurate compared with autoradiography. The purpose of this study was to investigate and correlate the hydrogen diffusion, hydrogen distribution and fracture surface on the environmental embrittlement of iron aluminides by electrochemical permeation measurement, hydrogen microprint technique and tensile test.

2. Experimental procedure

2.1. Materials

Alloy specimens were produced at Chung Shan Institute of Science and Technology. Six alloy ingots with nominal compositions (in at %) Fe-10Al, Fe-18Al, Fe-18Al-5Cr, Fe-28Al, Fe-28Al-5Cr, and Fe-40Al were prepared by repeated melting with vacuum induction melting (VIM) and then with vacuum arc remelting (VAR) and drop casting to form ingots. The ingots then were homogenized at 1100°C for 24 hours and followed by furnace cooling (cooling rate = 1°C/min). The chemical compositions of six specimens are list in Table I, and optical micrographs are shown in Fig. 1.

X-ray diffraction was used to determine B2 long-range order parameter [21] in this work. Their microstructures depend on aluminum content, those alloys containing $\leq$18 at % Al with α - disordered solid solution structure and those with $\geq$28 at % Al show B2 ordered structure. After etching in dilute aqua regia solution (10 ml HNO_3 + 30 ml HCl + 60 ml ethanol), Fe-18Al and Fe-28Al with 5 at % Cr both exhibit subgrain and all homogenized cast specimens show quite large grain size.

2.2. Electrochemical permeation

The instrumentation and procedures were similar to those described elsewhere [22]. The cathodic side, or hydrogen entry side, of the cell was galvanostatically polarized at a constant current density (10 mA/cm^2) in 0.1 N NaOH with 1 g/l of $Na_2S{\cdot}9H_2O$ added as a hydrogen recombination poison. The anodic side, or hydrogen exit side, of the cell was held at constant potential of 250 mV (SCE) in 0.1 N NaOH. The potentiostatic current gave a direct measure of the hydrogen flow rate. The cell assembly was immersed in a constant temperature bath maintained at 25 ± 1 °C.

Permeation specimens were fabricated to 40 × 30 × 0.5 mm sheets by electrical discharge machine (EDM), and then polished with grinding paper down to 1000 grit, finally finished with a thickness of 0.2 mm. The surfaces were rinsed with distilled water, cleaned ultrasonically in acetone, and dried quickly by warm air. The exit side of each specimen was electroplated with a thin nickel layer. The thickness of the nickel layer was 0.2 μm, so that the hydrogen permeation current density

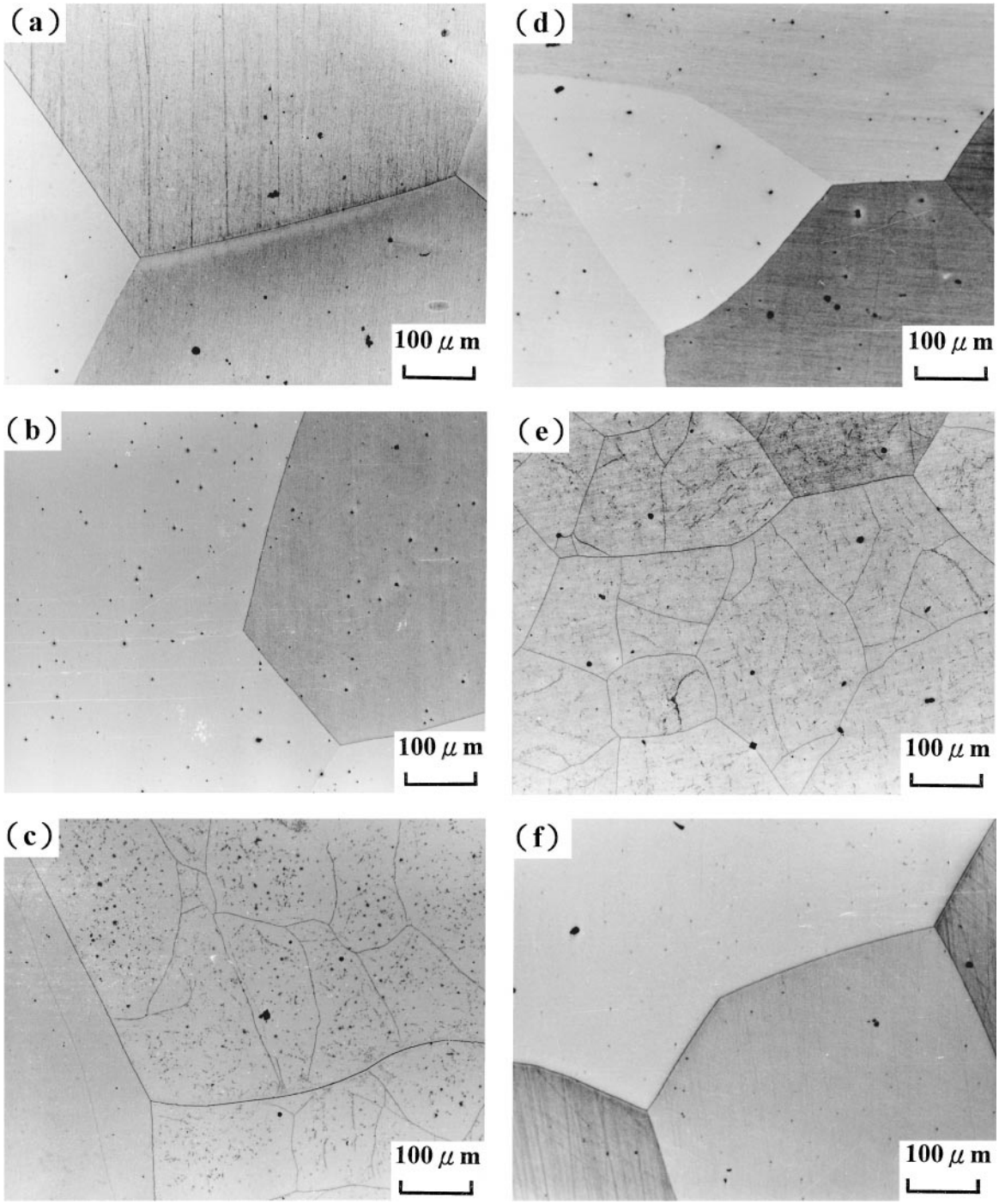

Figure 1 Microstructures of (a) Fe-10Al, (b) Fe-18Al, (c) Fe-18Al-5Cr, (d) Fe-28Al, (e) Fe-28Al-5Cr, and (f) Fe-40Al alloy.

TABLE I Chemical composition of iron alumnides (at %)

	Fe (at %)	Al (at %)	Cr (at %)
Fe-10Al	90.5	9.5	—
Fe-18Al	82.7	17.3	—
Fe-18Al-5Cr	76.2	18.8	5.0
Fe-28Al	72.1	27.9	—
Fe-28Al-5Cr	67.0	27.7	5.3
Fe-40Al	61.0	39.0	—

could be obtained correctly and the background current density minimized. Both sides of the membrane were deoxygenated. Permeation transients were recorded on a strip chart recorder.

For this study the flux of hydrogen through the specimen was measured in terms of the steady - state current density, i_p^∞ (mA/cm^2), and was converted to the steady - state hydrogen permeation flux, J_∞ (mol/m^{2}s), according to

$$J_\infty = \frac{i_p^\infty}{nF}, \tag{1}$$

where n is the number of electrons involved 1/mol and F is the Faraday's constant. The hydrogen permeation rate (mol/m^{2}s) is defined by

$$J_\infty L = \frac{i_p^\infty L}{nF}, \tag{2}$$

where L is the specimen thickness in mm. For diffusion as the rate - limiting step, the effective diffusivity, D_{eff} (m^2/s) is related to the time lag, t_L (s), by [23]

$$D_{\text{eff}} = \frac{L^2}{6t_L} \tag{3}$$

2.3. Hydrogen microprint technique

Experimental set - up for hydrogen microprint technique is quite similar to that used for permeation measurement [18, 19]. The cathodic charging side or hydrogen entry cell was also galvanostatically polarized at a constant charging current in 0.1 N NaOH. The hydrogen exit side was covered with liquid nuclear emulsion containing AgBr crystal as described by Overjero-Garcia [20]. Before coating with nuclear emulsion, the specimen surface was polished down to 0.05 μm alumina, and etched in dilute aqua regia for metallographic preparation. During cathodic charhging, hydrogen flux from the metal acted on the emulsion for the desired time causing the reduction of silver ions. Reactions in the exit side should be mainly:

$$H^{\circ} + Ag^{+} \rightarrow H^{+} + Ag^{\circ} \tag{4}$$

After a designed cathodic charging time, the specimen was removed and placed into a fixing solution at room temperature, then the specimen was washed with distilled water, dried and observed by scanning electron microscope (SEM). Some blank specimens with the same preparation but without hydrogen charging were also analyzed. The experimental procedures for the hydrogen microprint technique used in this study are metallographic preparation, nuclear emulsion coating, hydrogen charging with constant current density, fixing and SEM observation.

TABLE II Tensile test conditions

Pretreatment		1. Polished tensile testing specimens in vacuum furnace, 2. 300 °C, 2×10^{-7} torr, 4 hrs, 3. Furnace cooling to room temperature.
Test Conditions	Air	Test in air (RH = 65 ~ 75%)
	Vacuum Treatment	1. Drop into oil bath with a oil coating to prevent contact with air, 2. Test in air.
	Hydrogen Precharged	1. Cathodic charging in 0.1 N NaOH + 5 g/l $Na_2S{\cdot}9H_2O$ with a constant current density of 300 mA/cm^2 to the unmasked gauge area for 72 hrs, 2. Rinse with distilled water, 3. Dry with blowing air, 4. Dip with oil to prevent the specimen contact with air, 5. Test in air.

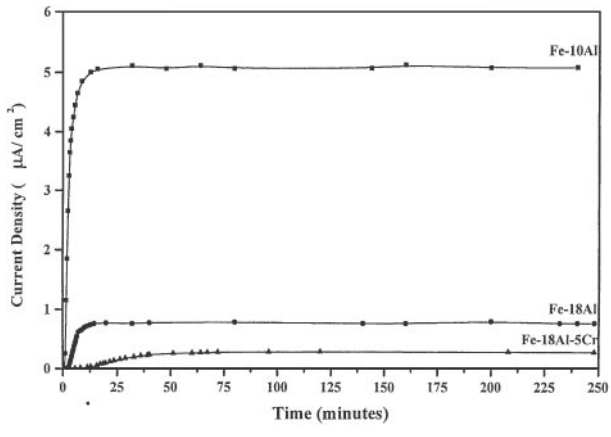

Figure 2 Permeation curves of three iron aluminides.

TABLE III Permeation data

Iron Aluminides	D_{eff} (m^2/s)	$J_{\infty}L$ (mol(H)/m·s)
Fe-10Al	6.95×10^{-10}	4.47×10^{-10}
Fe-18Al	3.46×10^{-10}	6.81×10^{-11}
Fe-18Al-5Cr	7.84×10^{-11}	2.52×10^{-11}
Fe-28Al	undetectable	undetectable
Fe-28Al-5Cr	undetectable	undetectable
Fe-40Al	undetectable	undetectable

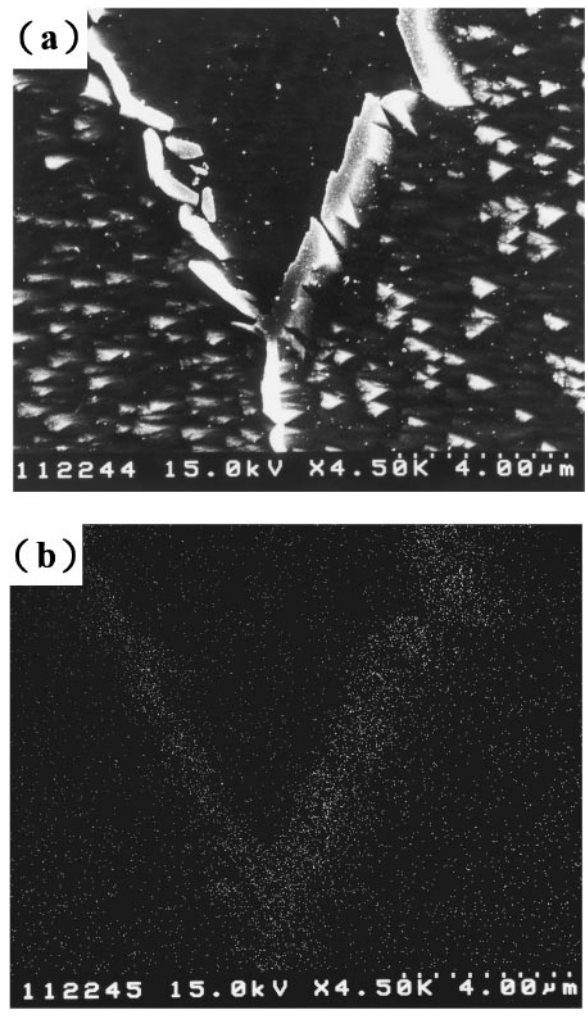

Figure 3 Fe-18Al-5Cr: (a) grain boundaries, (b) x-ray map showing Cr rich along grain boundaries.

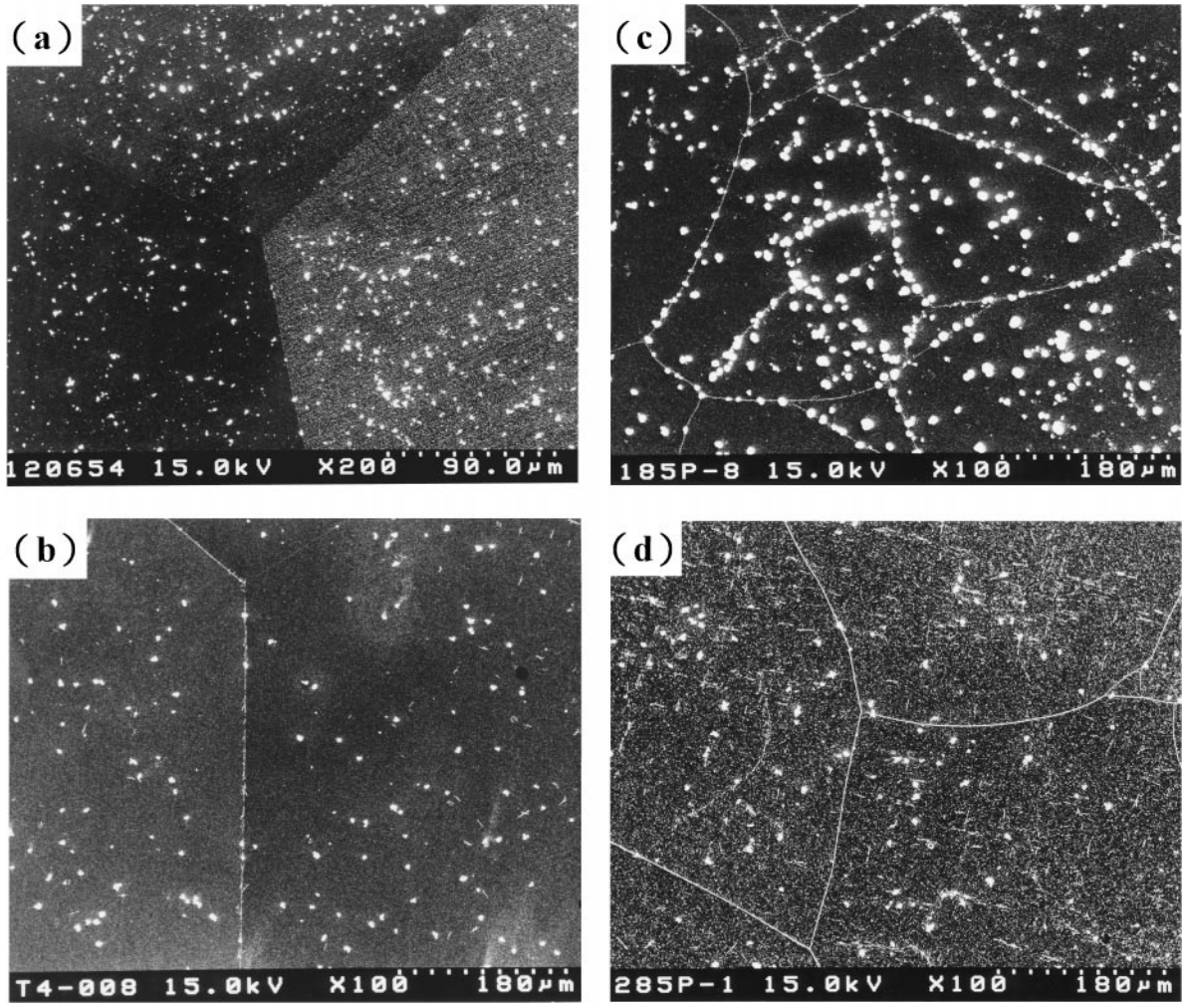

Figure 4 Surface of various specimens after cathodic charging with a constant current density (10 mA/cm^2) in 0.1 N NaOH solution at 25°C for (a) 15 minutes, Fe-10Al, (b) 15 minutes, Fe-18Al, (c) 60 minutes, Fe-18Al-5Cr, +3 g/l promoter in 0.1 N NaOH solution, (d) 240 minutes, Fe-28Al-5Cr, +3 g/l promoter in 0.1 N NaOH solution.

2.4. Tensile testing

The tensile specimens with gage section of $6 \times 4.4 \times 3$ mm were fabricated by EDM, and polished through 0.05 μm alumina. Tensile tests were conducted at room temperature at a strain rate of 2.0×10^{-4}/s in a Shimadzu AG – 250KNG tensile machine. Test environments included air, vacuum treatment and hydrogen precharged. The detailed testing conditions are designed as in Table II. The relative humidity (RH) of room air were varied from 65% to 75% and temperature range were 18 to 22 °C. After testing, the fracture surfaces were examined by SEM.

3. Results and discussion

3.1. Permeation test

Permeation curves for various iron aluminides are shown in Fig. 2. Permeation rate and diffusivity defined by Equations 1–3 are presented in Table III. The data clearly show a decrease in both $j_\infty L$ and D_{eff} as aluminum content increase for these alloys. No hydrogen diffusion has been detected through the thin specimens containing more than 28 at % Al which is due to Fe-Al intermetallic compounds acting as an obstacle to steady - state and unsteady - state transport.

The permeation curve also shows 5% Cr addition in Fe-18Al alloy lowering both permeation rate and diffusivity. In our permeation results, the effect of Al on hydrogen permeation appears to override the effect of Cr addition. Diffusivity decreases in Fe-18Al-5Cr due to the Cr segregation along grain boundaries. The higher Cr content (∼25 at %) on grain boundaries was confirmed by energy - dispersive spectrometer (EDX) and shown in Fig. 3.

Diffusivity in Fe-18Al was reported 10^{-11} m^2/s [16], and estimated 1.5×10^{-13} m^2/s [16] in Fe-25Al and 4.4×10^{-13} m^2/s [24] in Fe-40Al at room temperature by previously investigators using other measurement techniques. Our present results are in the same order of magnitude and good agreement with the limited work of others.

3.2. Hydrogen microprint technique

It was observed that reduced silver grains by hydrogen are gradually increased on various specimen surfaces after cathodic charging with a constant current density at room temperature and shown in Fig. 4a–d respectively. Silver grains are not presented in the blank specimens of various iron aluminides same as in Fig. 1. Silver grains are uniform throughout the grains and grain boundaries of Fe-10Al and Fe-18Al specimens in Fig. 4a and b. A distinct array of silver grains are visible at grain boundaries and subgrain boundaries in

TABLE IV Tensile property of various iron aluminides

Iron Aluminides	Test Environment	UTS (Mpa)*	Elongation (%)	Ductility Loss (%)**	Embrittlement Type
Fe-10Al	Air	299	63.4	4	Hydrogen
	Vacuum Treatment	323	66.1	—	Embrittlement
	Hydrogen Precharged	290	49.8	25	
Fe-18Al	Air	389	22.8	5	
	Vacuum Treatment	421	24	—	
	Hydrogen Precharged	193	13	46	
Fe-18Al-5Cr	Air	393	16.6	1	
	Vacuum Treatment	396	16.9	—	
	Hydrogen Precharged	377	21.3	14	
Fe-28Al	Air	92	8.3	50	Moisture
	Vacuum Treatment	331	16.6	—	Induced
	Hydrogen Precharged	366	15.4	7	Embrittlement
Fe-28Al-5Cr	Air	69	16.4	34	
	Vacuum Treatment	125	11.2	—	
	Hydrogen Precharged	157	11	2	
Fe-40Al	Air	68	16.1	57	
	Vacuum Treatment	247	16.7	—	
	Hydrogen Precharged	282	16	4	

*Ultimate Tensile Strength.

**Ductility Loss (%) $= \frac{\text{Elongation in Vacuum} - \text{Elongation in Air of Precharged}}{\text{Elongation in Vacuum}} \times 100\%$.

Fe-18Al-5Cr and Fe-28Al-5Cr after longer cathodic charging time in 1 N NaOH with 3 g/l promoter solution. So, the hydrogen transport in Fe-10Al and Fe-18Al is lattice and grain boundary diffusion which is same as in α-Fe. For Fe-18Al-5Cr and Fe-28Al-5Cr, the diffusion path is limited along grain boundaries, subgrain boundaries and periphery of precipitates on matrix. The fine silver grains located on Cr rich grain boundaries were analyzed and confirmed by EDX in Fig. 5. No silver grains are appeared in Fe-28Al and Fe-40Al after extremely high cathodic current density and long charging time. These results indicate the hydrogen permeation rate and diffusivity are extremely low in Fe-28Al and Fe-40Al due to B2 ordered structure of iron aluminide.

The higher diffusivity of Fe-10Al and Fe-18Al is due to lattice diffusion in bcc solid solution (α - disordered) structure, and more silver grains can be observed on specimen surface after shorter cathodic charging time. The permeation rate and diffusivity of hydrogen is strongly affected by diffusion paths and trapping sites. Microprint technique is well developed to observe hydrogen distribution, and detects the hydrogen diffusion paths and trapping sites accurately. More silver grains reduced during shorter cathodic charging time, which means higher hydrogen permeation rate and diffusivity in metals.

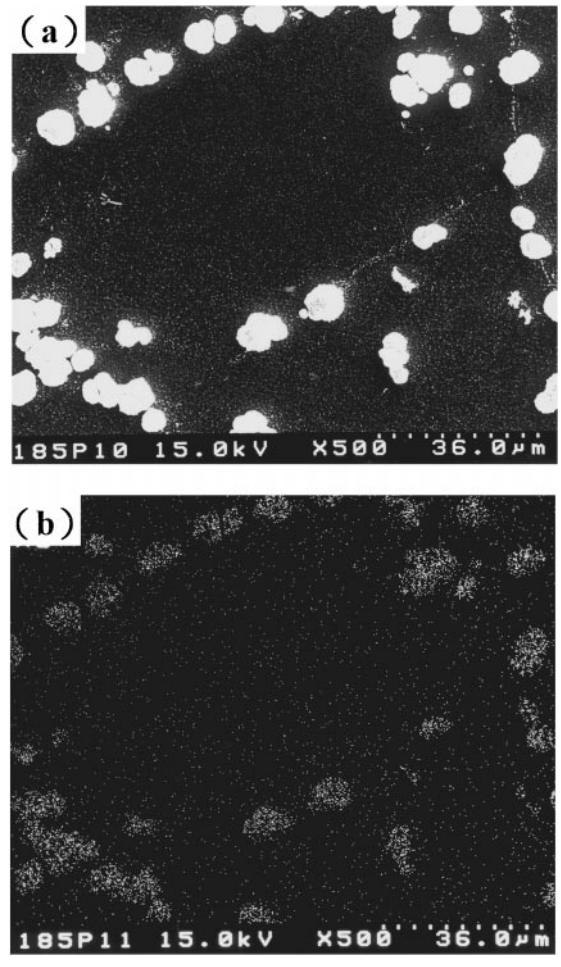

Figure 5 Fe-18Al-5Cr: (a) silver grains are visible at grain boundaries, (b) x-ray map showing Ag.

3.3. Tensile testing

The results of tensile tests in various environments are presented in Table IV. The hydrogen precharged Fe-10Al, Fe-18Al and Fe-18Al-5Cr showed significant degradation in elongation and strength. For tests conducted in air, Fe-28Al, Fe-28Al-5Cr and Fe-40Al exhibited most degradation in elongation and strength.

For the hydrogen precharged Fe-10Al specimen, is still mainly simple ductile fracture with a elongation of 49.8%, is shown in Fig. 6a, while the fractograph of precharged Fe-18Al and Fe-18Al-5Cr show transgranular fracture surface in Fig. 6b and c respectively. This result indicates that Fe-18Al and Fe-18Al-5Cr are more susceptible to hydrogen degradation.

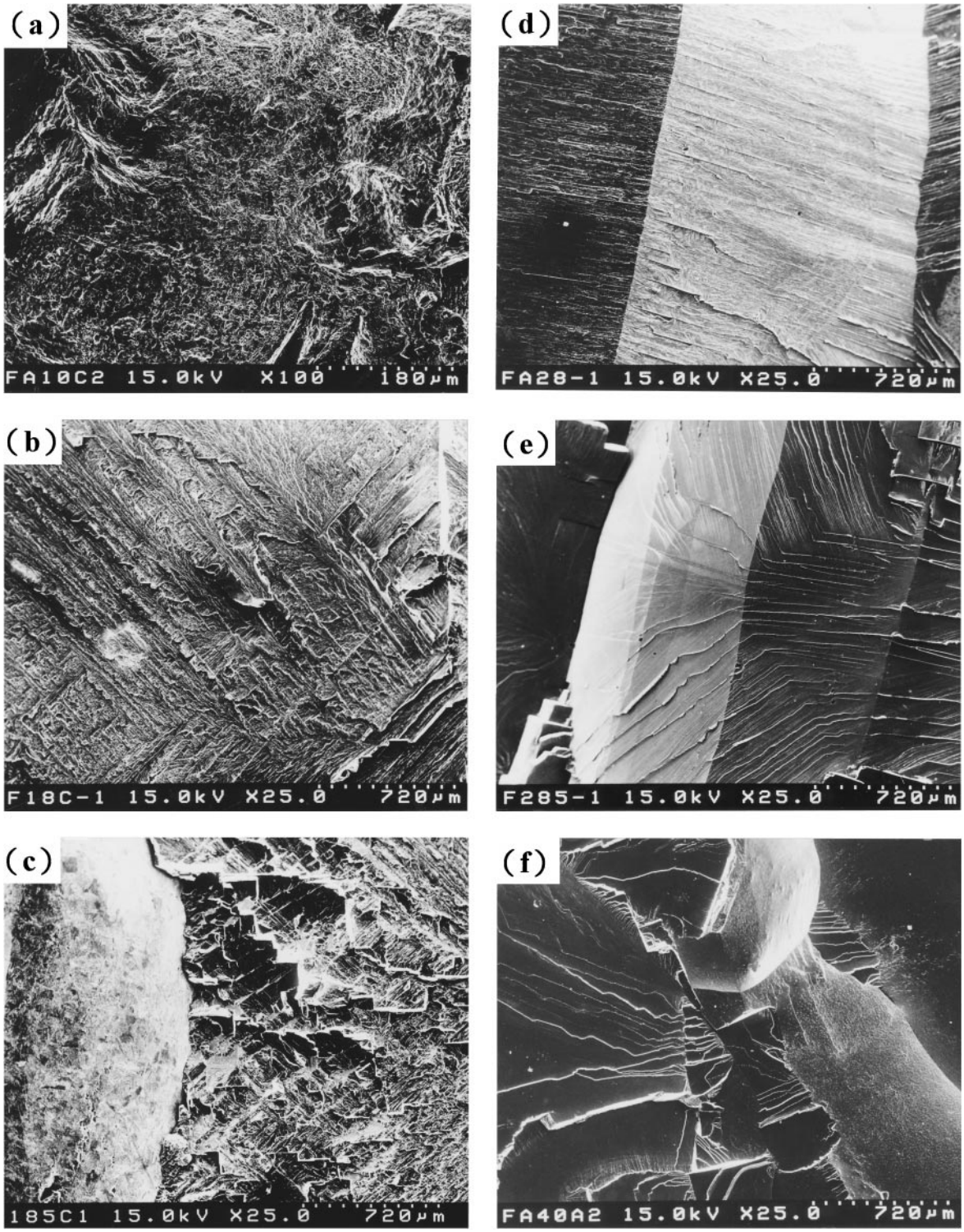

Figure 6 Fracture surfaces of (a) Fe-10Al, (b) Fe-18Al and (c) Fe-18Al-5Cr with hydrogen precharging, (d) Fe-28Al, (e) Fe-28Al-5Cr, and (f) Fe-40Al in air.

For iron aluminides containing ≥28 at % Al, the ductility was slightly influenced with hydrogen precharging, but significantly loss in air. Fe-28Al and Fe-28Al-5Cr specimens test in air both show transgranular cleavage fracture in Fig. 6d and e respectively, while Fe-40Al shows intergranular fracture. Moisture induced hydrogen embrittlement has been reported as one of the most possible embrittlement mechanisms of the brittleness in intermetallics. Segregation of moisture induced hydrogen atoms at the crack tip, lowering the bonding strength, and cause transgranular cleavage or intergranular fracture. The permeation rate and diffusivity of iron aluminides is extremely low and undetectable by electrochemical permeation measurement in this study. Intermetallic compounds considered as an obstacle (antitrap) to reduce hydrogen diffusion path, The susceptibility of iron aluminides (≥28 at % Al) to moisture is much stronger than to hydrogen environment.

Therefore, moisture induced embrittlement of iron aluminides is not essentially related to either the diffusivity or permeation rate of hydrogen but related to

the critical amount of hydrogen generated at the crack tip. The most practical method to alleviate moisture induced embrittlement of iron aluminides is suggested to eliminate the hydrogen generation on metal surface.

4. Conclusions

Synthesizing the results and discussion of these systematic experiments, there are some conclusions described below:

1. From the data of the permeation and tensile tests, the iron aluminides containing $\leq$18 at % Al are more susceptible to hydrogen embrittlement than iron aluminides ($\geq$28 at % Al). Iron aluminides ($\geq$28 at % Al) are susceptible to chemisorption of moisture in air, and induce embrittlement in ordered structure of iron aluminides.

2. Due to extremely low hydrogen permeation rate and diffusivity in iron aluminides, the embrittlement mechanism can be concluded as moisture induced hydrogen embrittlement.

3. To protect iron aluminides from moisture induced embrittlement, coating to prevent contact with air is a feasible method.

Acknowledgements

The authors are grateful for the support of this research by the National Science Council, Republic of China under Contract No. NSC 88 - 2216 - E019 - 004. The authors also thank Dr. C. T. Liu of Oak Ridge National Laboratory, Prof. P. Y. Lee, Dr. J. P. Chu and Mr. J. H. Wu of National Taiwan Ocean University, Dr. C. Y. Ma and Mr. C. S. Chen of Materials R&D Center at Chung Shan Institute of Science and Technology for their technical assistance and helpful comments.

References

1. C. G. McKAMEY, J. H. DeVAN, P. F. TORTORELLI and V. K. SIKKA, *J. Mater. Res.* **6** (1991) 1779.
2. N. S. STOLOFF and C. T. LIU, *Intermetallics* **2** (1994) 75.
3. Y. F. ZHU, C. T. LIU and C. H. CHEN, *Scr. Mater.* **35** (1996) 1435.
4. C. T. LIU, J. L. WRIGHT and N. S. STOLOFF, *ibid.* **38** (1998) 1601.
5. M. INOUE, K. SUGANUMA and K. NIIHARA, *Ibid.* **39** (1998) 1477.
6. K. YOSHIMI and S. HANADA, *J. Metals* **49** (1997) 46.
7. P. BANERJEE and R. BALASUBRAMANIAM, *Scr. Mater.* **38** (1998) 1143.
8. N. S. STOLOFF and D. J. DUQUETTE, *J. Metals* **43** (1993) 30.
9. A. BAHADUR and O. N. MOHANTY, *J. Mater. Sci.* **26** (1991) 2685.
10. R. J. LYNCH, W. W. MILIGAN and L. A. HELDT, in Parkins Symposium on Fundamental Aspects of Stress Corrosion Cracking, TMS, Warrendale, USA, 1992, p. 117.
11. J. P. TU, L. MENG and M. S. LIU, *Scr. Mater.* **38** (1998) 833.
12. P. BANERJEE and R. BALASUBRAMANIAM, *ibid.* **39** (1998) 1215.
13. I. R. ROBERTSON and D. TETER, *J. Metals* **48** (1996) 55.
14. X. Y. CHENG and X. J. WAN, *Scr. Mater.* **38** (1998) 1215.
15. L. M. PIKE and C. T. LIU, *ibid.* **38** (1998) 1475.
16. H. HOSODA, K. MIZUUCHI and K. INOUE, *J. Metals* **49** (1997) 56.
17. C. L. FU and G. S. PAINTER, *J. Mater. Res.* **6** (1991) 719.
18. W. C. LUU and J. K. WU, *Materials Letters* **24** (1995) 175.
19. *Idem., Corrosion Sci.* **38** (1996) 239.
20. J. OVERJERO-GARCIA, *J. Mater. Sci.* **20** (1985) 2623.
21. C. G. McKAMEY, in "Physical Metallurgy and Processing of Intermetallic Compounds" (Chapman & Hall, New York, 1994) p. 351.
22. R. D. McCRIGHT, Ph. D. Thesis, The Ohio State University, Columbus, OH, 1971.
23. J. CRANK, in "The Mathematics of Diffusion" (Oxford University Press, Oxfrd, 1977) p. 44.
24. Y. YANG and S. HANADA, *Scr. Metall. Mater.* **32** (1995) 1719.

Received 24 June 1999
and accepted 3 February 2000